A green ultrasound-assisted access to some new 1-benzyl-3-(4-phenoxybutyl) imidazolium-based ionic liquids derivatives – potential corrosion inhibitors of mild steel in acidic environment

M. Messali* and M.A.M Asiri

Chemistry Department, Faculty of Science, Taibah University, Al Madinah Al Mounawara, 30002 Saudi Arabia.

This article is dedicated to our Prof Dr Abdulrahman Mohammed Al-Muneer

Abstract

A green ultrasound-assisted synthesis and caracterization of two new ionic liquids derivatives namely, 1-benzyl-3-(4-phenoxybutyl)-1H-imidazol-3-ium bromide (MA1) 1-benzyl-3-(4-phenoxybutyl)-1H-imidazol-3-ium tetrafluoroborate (MA2) is described and their inhibitive action against the corrosion of C-steel in 1.0 M HCl solution were investigated. The corrosion rate of steel decreased both in the presence of these two molecules. Their inhibition efficiencies increase with the inhibitor concentration to reach 94.6 and 97.6% at 10^{-2} M of MA1 and MA2, respectively. The adsorption of these compounds on C-steel surface agrees Langmuir's adsorption isotherm. The free enthalpy related to the adsorption process reveals the mode inhibitors adsorption. Quantum chemical approach, using the density functional theory (DFT), was applied in order to get better understanding about the relationship between the inhibition efficiency and molecular structure of MA1 and MA2. The calculated quantum chemical parameters include the highest occupied molecular orbital (HOMO), lowest unoccupied molecular orbital (LUMO), dipole moment and amount of electrons transferred. The results of the study suggest that MA1 is a better corrosion inhibitor than MA2, which is in agreement with most experimental findings obtained at different concentrations.

Keywords: Green procedure, Ultrasonic irradiation, imidazolium-based ionic liquids, corrosion Inhibitors, Acid, Quantum chemical parameters.

1. Introduction

Corrosion is an electrochemical process by which the metallic structures are destroyed gradually through anodic dissolution [1]. Therefore, the consumption of inhibitors to reduce corrosion has increased in recent years. The corrosion controls by inhibitors is one of the most common effective and economic methods to protect metals in acid media [2–16].

Electronegative functional groups and л-electron in triple or conjugated double bonds as well as heteroatoms like sulphur, phosphorus, nitrogen and oxygen are major adsorption centres. The modes of adsorption depend on (i) the chemical structure of the molecule, (ii) the chemical composition of the solution, (iii) the nature of the metal surface and (iv) the electrochemical potential of the metal-solution interface. The most important aspect of inhibition, normally considered by corrosion scientists is the relation between the molecular structure and corrosion inhibition efficiency [17-19].
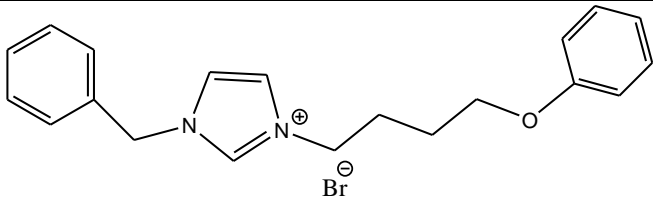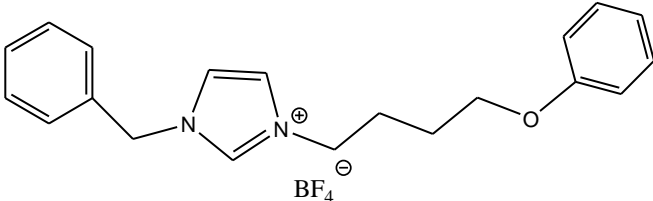
Ionic liquids (ILs) are emerging as smart and excellent solvents, which are made of positive and negative ions that pack so poorly together that they are liquids near room temperature.[20-22] They offer significant properties such as negligible vapor pressure, high thermal stability, lack of inflammability, decent solubility for organic, inorganic and organometallic compounds, non-coordinating but good solvating ability, high ionic conductivity, and a wide electrochemical potential

window [23-29]. Apart from these features each IL shows unique chemical and physical property by proper varying its cation and anion [30].

Recently, Imidazolium and pyridinium compounds are reported to show corrosion resistant behavior on copper [31,32], mild steel [33-39] and aluminum [40]. It was found that the action of such inhibitors depends on the specific interaction between the functional groups and the metal surface, due to the presence of the –C=N- moiety and electronegative nitrogen in the molecule.

In the same context, Herein, we will report the synthesis and characterization of two new N-alkylpyridazinium ionic liquids namely, 1-benzyl-3-(4-phenoxybutyl)-1H-imidazol-3-ium bromide (**MA1**) and 1-benzyl-3-(4-phenoxy butyl)-1H-imidazol-3-ium tetrafluoroborate (**MA2**), with the aim gravimetrically to study applicability as corrosion inhibitors for carbon steel in 1.0 M HCl. The chemical structures of the studied pyridazinium ionic liquids are given in Table1.

Table 1. The chemical structure of the studied imidazolium-based ionic liquids.

Compound	Structural formula	Molar mass
MA1		387.31
MA2		394.21

2.   Experimental methods
2.1.   Synthesis
2.1.1. Materials

The steel used in this study is a carbon steel (Euronorm: C35E carbon steel and US specification: SAE 1035) with a chemical composition (in wt%) of 0.370 % C, 0.230 % Si, 0.680 % Mn, 0.016 % S, 0.077 % Cr, 0.011 % Ti, 0.059 % Ni, 0.009 % Co, 0.160 % Cu and the remainder iron (Fe). The carbon steel samples were pre-treated prior to the experiments by grinding with emery paper SiC (120, 600 and 1200); rinsed with distilled water, degreased in acetone in an ultrasonic bath immersion for 5 min, washed again with bidistilled water and then dried at room temperature before use.

The acid solutions (1.0 M HCl) were prepared by dilution of an analytical reagent grade 37 % HCl with double-distilled water. The concentration range of **MA1** and **MA2** employed was 10^{-6} M to 10^{-2} M. The reagents: imidazole (98%), benzyl bromide (97%) and 4–phenoxybutyl bromide (98%), were purchased from Aldrich and used as received. All solvents were of HPLC grade.

2.1.2.   Measurements and equipments

All new compounds were synthesized and characterized by ^{1}H NMR, ^{13}C NMR, IR, and LCMS. ^{1}H NMR (400 MHz) and ^{13}C NMR (100 MHz) spectra were measured in DMSO at room temperature. Chemical shifts (δ) were reported in ppm to a scale calibrated for tetramethylsilane (TMS), which is used as an internal standard. The LCMS spectra were measured with a Micromass, LCT mass spectrometer. IR spectra were recorded in NaCl disc on a Schimadzu 8201 PC, FTIR

spectrophotometer (ν_{max} in cm^{-1}). The ultrasound-assisted reactions were performed using a controllable laboratory ultrasonic bath.

2.1.3. Synthesis of 1-benzyl-3-(4-phenoxybutyl)-1H-imidazol-3-ium bromide (MA1) under Ultrasonic irradiation

N-benzylimidazole (1 eq) and the 4–phenoxybutyl bromide (1eq) were placed in a closed container and exposed to irradiation for 5 hours at 70 ºC using a sonication bath. Completion of the reaction was marked by the precipitation of a solid from the initially obtained clear and homogenous mixture in toluene. The product is isolated by filtration and washed three times with Ethyl acetate to remove any unreacted starting materials and solvent. Subsequently, the imidazolium salt was washed with ethyl acetate. In each case, the IL was finally dried at a reduced pressure to remove all volatile organic compounds. White crystals, yield 79%, mp 153-155 ºC; ^{1}H NMR (400MHz, CDCl$_3$) δ: 1.77 (quint, $J = 8$ Hz, 2H), 2.07 (quint, $J = 8$ Hz, 2H), 3.91 (t, $J = 8$ Hz, 2H), 4.35 (t, $J = 8$ Hz, 2H), 5.52 (s, 2H), 6.77-6.88 (m, 3H), 7.17-7.55 (m, 9H), 10.45 (s, 1H). ^{13}C NMR (100MHz, CDCl$_3$) δ: 158.6 (C), 135.5 (CH), 133.0 (C), 129.5 (CH), 129.4 (CH), 129.4 (CH), 128.9 (CH), 122.6 (CH), 122.2 (CH), 120.8 (CH), 114.4 (CH), 66.7 (CH$_2$), 53.2 (CH$_2$), 49.7 (CH$_2$), 26.9 (CH$_2$), 25.7 (CH$_2$). IR (ν_{max} cm^{-1}) 3132 (C-H, sp^2), 1599-1471 (C=C), 1165(C-N), 1082 (C-O), LCMS (M-Br) 307 found for C$_{20}$H$_{23}$N$_2$O$^+$.
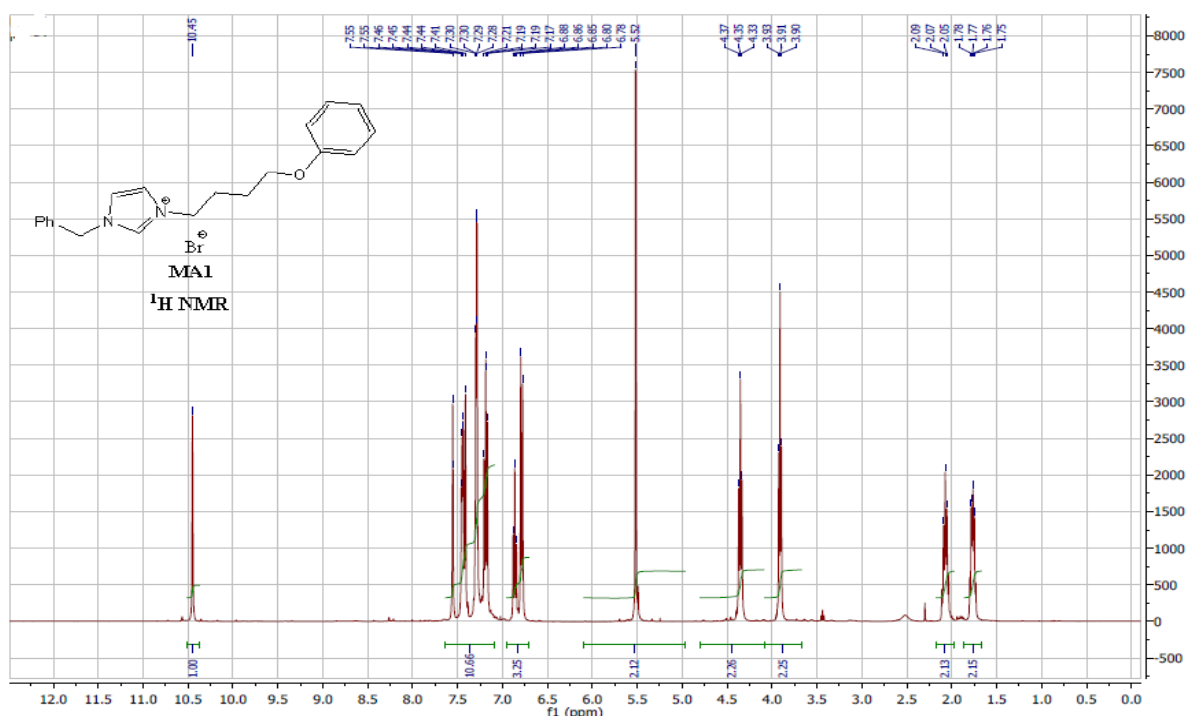

Fig 1. ^{1}H NMR spectrum (CDCl$_3$) of 1-benzyl-3-(4-phenoxybutyl)-1H-imidazol-3-ium bromide (MA1)

2.1.4. Synthesis of 1-benzyl-3-(4-phenoxybutyl)-1H-imidazol-3-ium tetrafluoroborate (MA2) under Ultrasonic irradiation

Imidazolium bromide (1eq) and NaBF$_4$ (1,1eq) in a small amount of acetonitrile were placed in a closed container and exposed to irradiation for 1 hours at 70 ºC using a sonication bath. The cooled reaction mixture was filtered through Celite to remove solid metal halide. The evaporation of acetonitrile leaded quantitatively to the desired ionic liquids.

Brown crystals, yield 91%, mp 89-92 ºC. 1H NMR (400MHz, CDCl3) δ: 1.72 (quint, $J = 8$ Hz, 2H), 2.01 (quint, $J = 8$ Hz, 2H), 3.89 (t, $J = 8$ Hz, 2H), 4.20 (t, $J = 8$ Hz, 2H), 5.28 (s, 2H), 6.80-6.91 (m, 3H), 7.19-7.37 (m, 9H), 8.97 (s, 1H). ^{13}C NMR (100MHz, CDCl$_3$) δ: 158.6 (C), 135.5 (CH), 133.0 (C), 129.5 (CH), 129.4 (CH), 129.4 (CH), 128.9 (CH), 122.6 (CH), 122.2 (CH), 120.8 (CH), 114.4 (CH), 66.7 (CH$_2$), 53.2 (CH$_2$), 49.7 (CH$_2$), 26.9 (CH$_2$), 25.7 (CH$_2$). ^{19}F NMR (377 MHz, CDCl$_3$) δ: -150.11;

IR (ν_{max} cm^{-1}) 3131 (C-H, sp^2), 1598-1470 (C=C), 1163(C-N), 1080 (C-O); LCMS (M-BF$_4$) 307 found for C$_{20}$H$_{23}$N$_2$O$^+$.
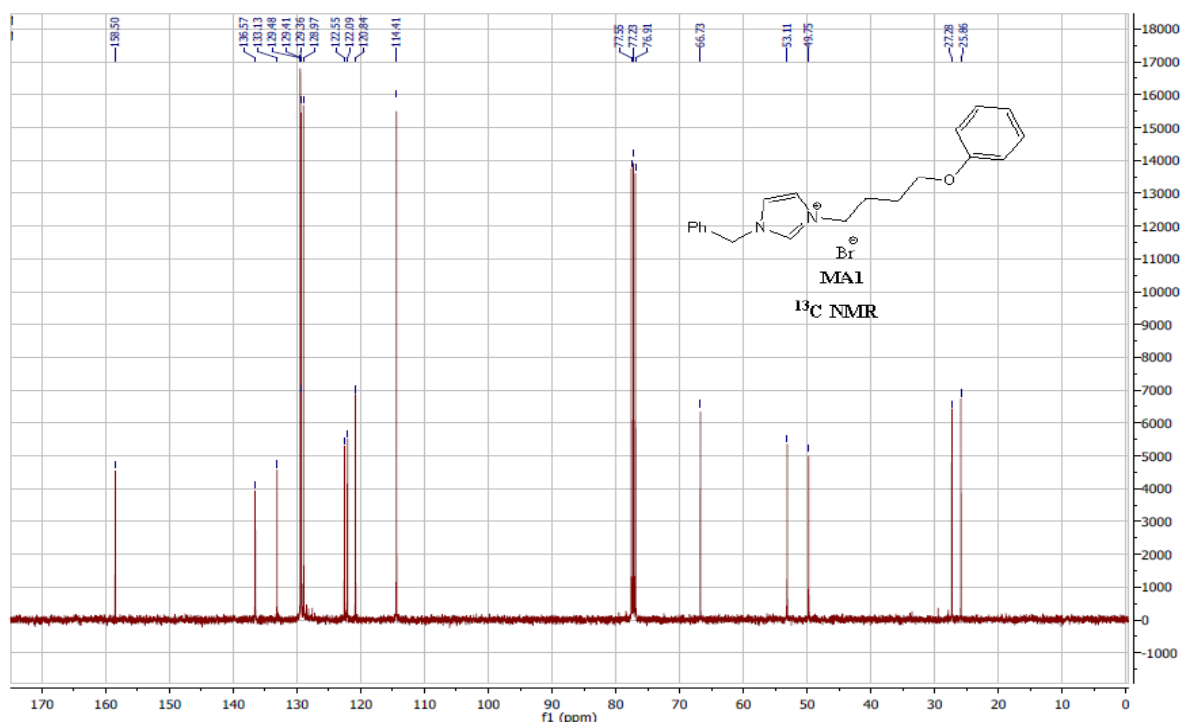

Fig 2. ^{13}C NMR spectrum (CDCl$_3$) of 1-benzyl-3-(4-phenoxybutyl)-1H-imidazol-3-ium bromide (MA1)
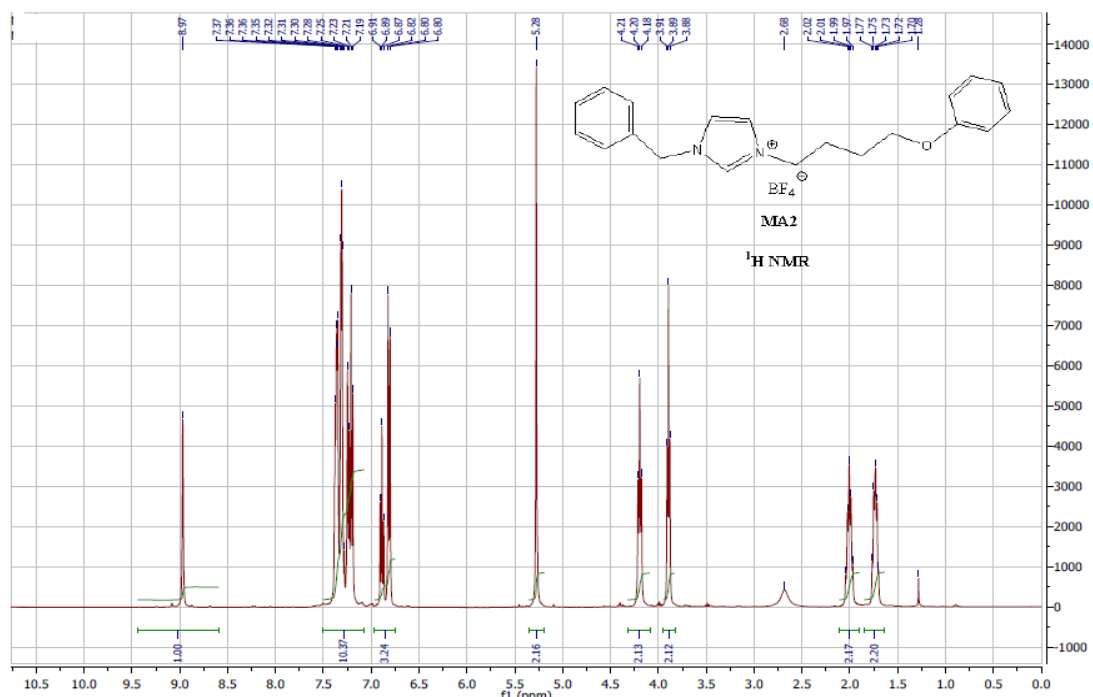

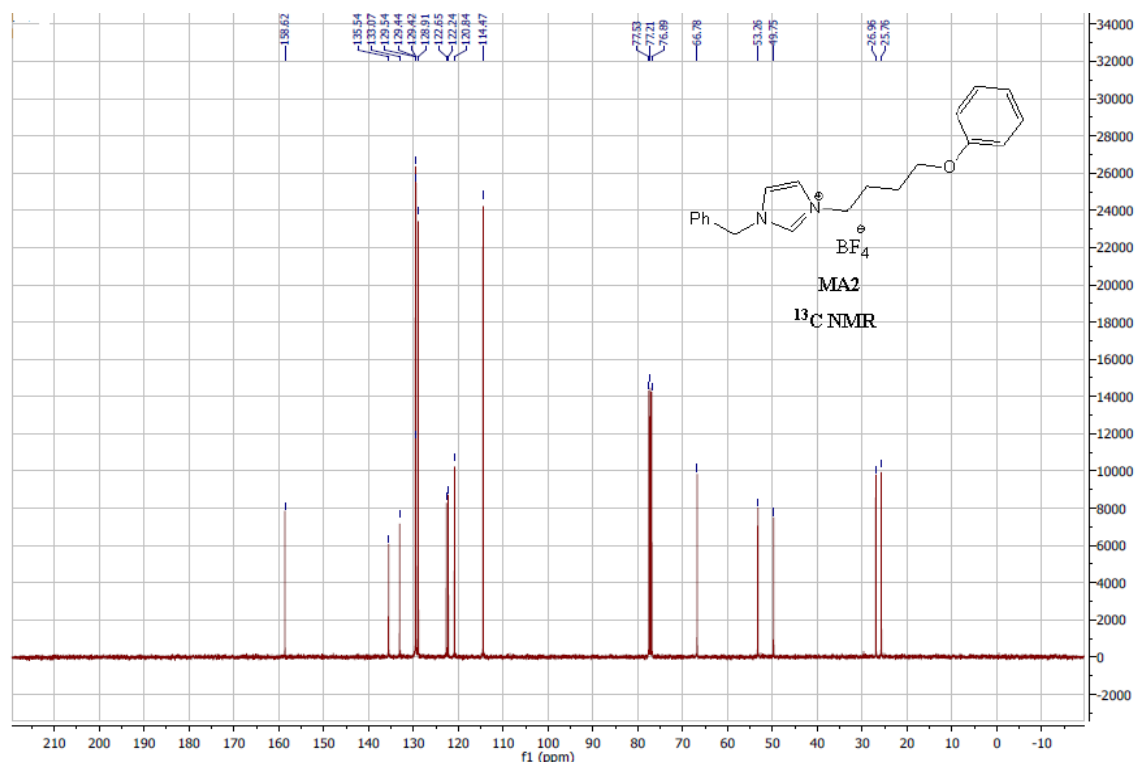**Fig 3**. ^{1}H NMR spectrum (CDCl$_3$) of 1-benzyl-3-(4-phenoxybutyl)-1H-imidazol-3-ium tetrafluoroborate (MA2)

Fig 4. ^{13}C NMR spectrum (CDCl$_3$) of 1-benzyl-3-(4-phenoxybutyl)-1H-imidazol-3-ium tetrafluoroborate (MA2)
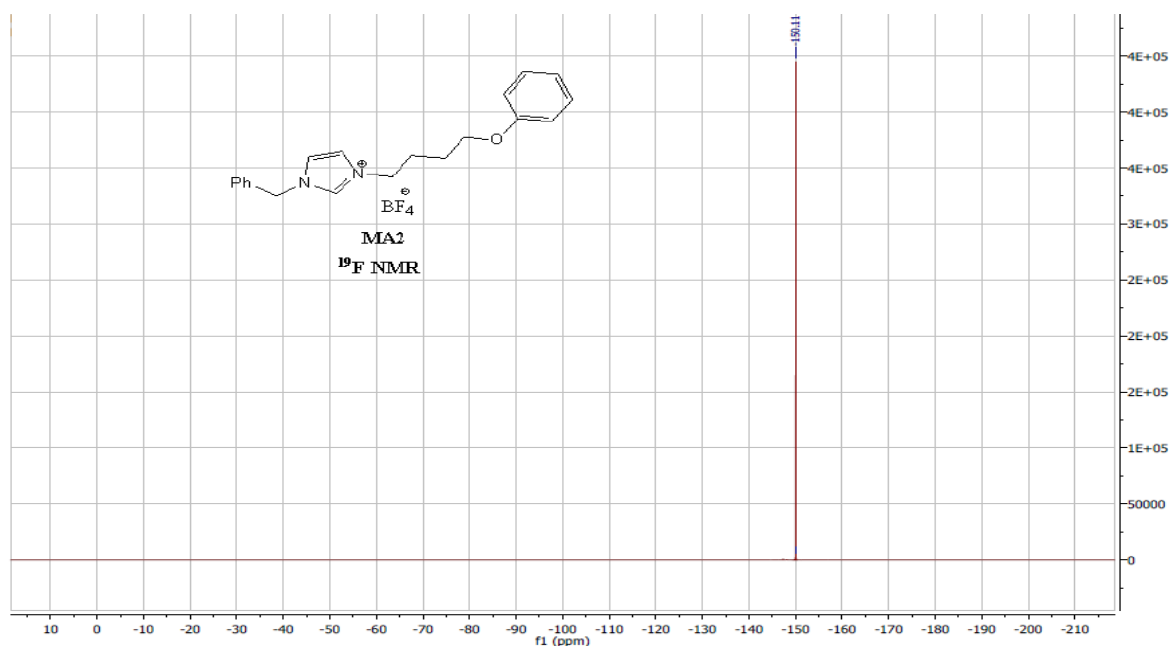

Fig 5. ^{19}F NMR spectrum (CDCl$_3$) of 1-benzyl-3-(4-phenoxybutyl)-1H-imidazol-3-ium tetrafluoroborate (MA2)

2.2.   Weight loss measurements

The gravimetric measurements were carried out at the definite time interval of 4 h at room temperature using an analytical balance (precision ± 0.1 mg). The carbon steel specimens used have a rectangular form (1.6 x 1.6 x 0.07 cm). Gravimetric experiments were carried out in a double glass cell equipped with a thermostatic cooling condenser containing 50 mL of non-de-aerated test solution. After immersion period, the steel specimens were withdrawn, carefully rinsed with doubly distilled water, ultrasonic cleaning in acetone, dried at room temperature and then weighted. Triplicate experiments were performed in each case and the mean value of the weight loss is calculated.

2.3. Computational approach

All geometry optimizations and quantum chemical calculations were performed using density functional theory (DFT) because it is a trade-off between computational cost, the complexity of the ionic liquids studied, the selected molecular properties to be calculated and reasonability of the desired results. The Becke's Three Parameter Hybrid Functional using the Lee-Yang-Parr correlation functional theory (B3LYP) was selected for the calculations [41–43]. Calculations were done with the 6-31+G(d,p) basis set. The addition of diffuse functions is considered important for a good description of ionic systems with 6- 31G* basis set is implemented in Gaussian 03 program package [44]. This approach is shown to yield favorable geometries for a wide variety of systems. The following quantum chemical parameters were calculated from the obtained optimized molecular structure: the energy of the highest occupied molecular orbital (E_{HOMO}), the energy of the lowest unoccupied molecular orbital (E_{LUMO}), the energy band gap ($\Delta E_{gap} = E_{HOMO} - E_{LUMO}$), the dipole moment ($\mu$) and the total energy (TE).
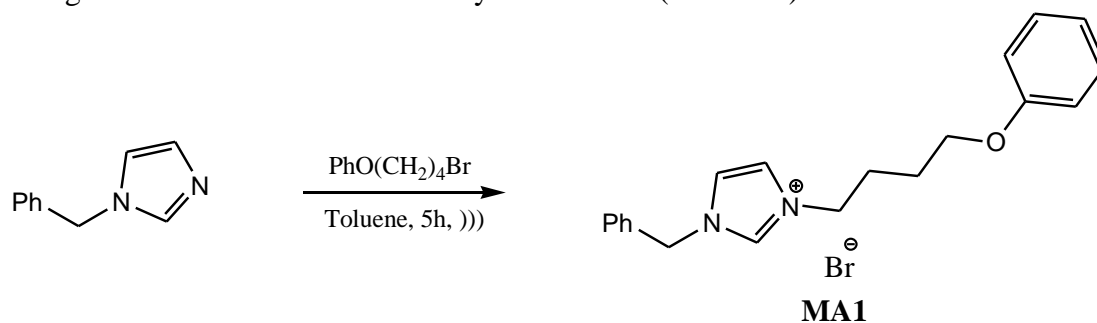
3.   Results and Discussion

3.1. Ultrasonic assisted synthesis of new benzylimidazolium-based ionic liquids

A number of procedures are ~~is~~ recommended for Green Chemistry, which may involve solvent-free reactions or non-classical modes of activation such as ultrasounds or microwaves [45]. The use of these technologies leads to large reductions in reaction times and enhancements in conversions, sometimes in selectivity, with several advantages of the eco-friendly approach. [46-51].
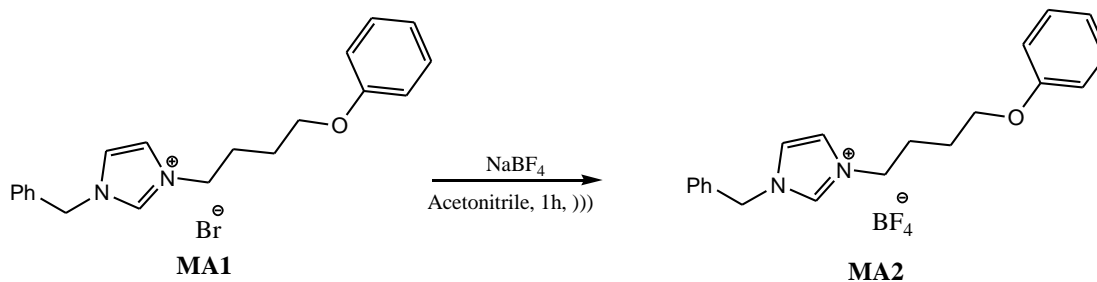
As part of our research objectives, new environmentally friendly pyridazinium-based ionic liquids (MA1, MA2) were prepared for the first time by using ultrasound irradiation in short reaction time and with good yields**.**

The nucleophilic alkylation of benzyimidazole with 4–phenoxybutyl bromide afforded the corresponding imidazolium bromide in 79% yield as solid. (scheme 1)

Scheme 1. N-alkylation of benzylimidazole under ultrasonic irradiation.

An alternative anion was subsequently introduced by a metathesis reaction with slight excess of sodium tetrafluoroborate (Scheme 2). The pure product was obtained after filtration of the sodium bromide, followed by evaporation of the filtrate and washing the residue with dichloromethane, followed by further filtration to remove the excess salt (NaBF₄). Finally, evaporation of the filtrate afforded the desired ionic liquid MA2 in 91% yield.

Scheme 2. Methathesis reaction under ultrasonic irradiation .

The ultrasound–assisted preparation of these new imidazolium-based ionic liquids was explored with the objective of shortening the reaction time.

3.2.   Effect of inhibitors concentration

Weight loss of C-steel, in mg cm^{-2} of the surface area, was determined at different concentration in the absence and presence of the new ionic liquids derivatives (MA1 and MA2) at 298K. From the weight loss results, the corrosion rate (C_R), the inhibition efficiency ($\eta_{WL}(\%)$) of the inhibitor and the degree of surface coverage (θ) were calculated using equations 1, 2 and 3 [52, 53].

$$C_R = \frac{W_b - W_a}{At} \tag{1}$$

$$\eta_{WL}(\%) = \left(1 - \frac{w_i}{w_0}\right) \times 100 \tag{2}$$

$$\theta = 1 - \frac{w_i}{w_0} \tag{3}$$

where W_b and W_a are the specimen weight before and after immersion in the tested solution, w_0 and w_i are the values of corrosion weight losses of carbon steel in uninhibited and inhibited solutions, respectively, A the total area of the carbon steel specimen (cm^2) and t is the exposure time (h) and θ is the degree of surface coverage of the inhibitor.

Table 2: Gravimetric results of mild steel in 1M HCl without and with addition of inhibitors at 298 K, The exposure time is 4h.

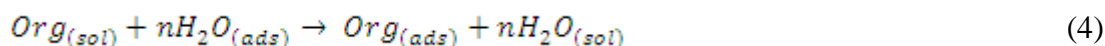| Inhibitors	Concentration (M)	$10^{-4} C_R$ (mg.cm^{-2} .h^{-1})	$\eta_{WL}(\%)$	θ
	Blank	0.290	--	--
MA1	10^{-6}	0.263	9.3	0.093
	10^{-5}	0.0628	78.3	0.783
	10^{-4}	0.0190	93.4	0.934
	10^{-3}	0.0185	93.6	0.936
	10^{-2}	0.0157	94.6	0.946
MA2	10^{-6}	0.239	17.5	0.175
	10^{-5}	0.1226	57.7	0.577
	10^{-4}	0.0675	76.7	0.767
	10^{-3}	0.0342	88.2	0.882
	10^{-2}	0.0069	97.6	0.976

The values of $\eta_{WL}(\%)$ for two inhibitors are given in Table 2. This show that the inhibition efficiency increases with the increasing inhibitor concentration. These results reveal that the compounds under investigation are fairly efficient inhibitors for C-steel dissolution in 1.0 M HCl solution. The inhibition of corrosion of C-steel by new ionic liquids derivatives can be explained in terms of adsorption on the metal surface.

These compounds can be adsorbed on the C-steel surface by the interaction between lone pairs of electrons of nitrogen atoms of the inhibitors and the metal surface. This process is facilitated by the presence of vacant orbital of low energy in iron atom, as observed in the transition group elements. Careful inspection of these results showed that, the ranking of the inhibitors according to $\eta_{WL}(\%)$ is as follows: MA1 > MA2 for the same concentration except for $c=10^{-2}$ where the efficiency of MA2 is slightly superior than MA2.

3.3. Adsorption isotherm and thermodynamic parameters

Basic information on the interaction between inhibitors and metal surface can be provided using the adsorption isotherms [54]. The adsorption of an organic adsorbate at metal–solution interface can occur as a result of substitutional adsorption process between organic molecules presented in the aqueous solution ($Org_{(sol)}$), and the water molecules previously adsorbed on the metallic surface ($H2O_{(ads)}$) [55]:

where $Org_{(sol)}$ and $Org_{(ads)}$ are the organic species in the bulk solution and adsorbed one on the metallic surface, respectively, $H_2O_{(ads)}$ is the water molecule adsorbed on the metallic surface and n is the size ratio representing the number of water molecules replaced by one organic adsorbate. In order to obtain the adsorption isotherm, the degree of surface coverage, θ, for different concentrations of inhibitor in 1.0 M HCl solutions has been evaluated by the equation (4).

$$Org_{(sol)} + nH_2O_{(ads)} \rightarrow Org_{(ads)} + nH_2O_{(sol)} \qquad (4)$$

Attempts were made to fit values of θ to many isotherm including Langmuir, Temkin Frumkin and Freundlich. The organic compound seems that follows well the Langmuir adsorption isotherm written in the rearranged form [56]:

$$\frac{C}{\theta} = \frac{1}{K} + C \text{ with } K = \frac{1}{55.5}\exp(-\frac{\Delta G^{\circ}_{ads}}{RT}) \qquad (5)$$

where C is the inhibitor concentration, K is the adsorption equilibrium constant, ΔG°_{ads} is the standard free energy of adsorption, 55.5 is the concentration of water in the solution in mol dm^{-3}, R is the universal gas constant and T is the absolute temperature in Kelvin. The relationship between C/θ and C presents linear behaviour at all temperatures studied (Fig. 6) with slopes equal to unity
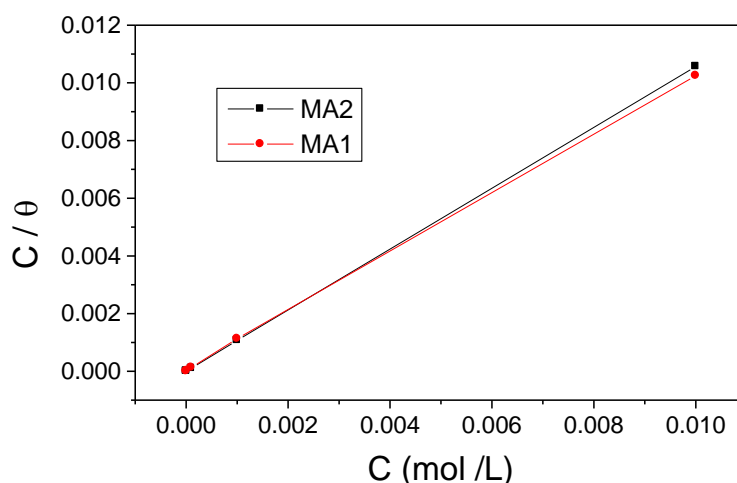
Fig 6. Langmuir isotherm of steel in the 1M HCl in presence of MA1 and MA2 .

All the obtained thermodynamic parameters are shown in Table 3. The negative values of $\Delta G°_{ads}$ for MA1 and MA2 indicate the spontaneous of the adsorption of this inhibitors and stability of the adsorbed layer on the sleel surface. More negative value designates that inhibitors are strongly adsorbed on the steel surface. Literature pointed that values of $\Delta G°_{ads}$ around -20 kJ.mol^{-1} or lower are related to the electrostatic interaction between the charged molecules and the charged metal (physisorption); those around -40 kJ.mol^{-1} or higher involve charge sharing or transfer from organic molecules to the metal surface to form a coordinate type of bond (chemisorption) [57-59]. The obtained values of $\Delta G°_{ads}$ surrounded -40 kJ.mol^{-1} indicating, that the adsorption mechanism of the imidazolium-based ionic liquids tested on steel in 1M HCl solution was of physical and chemical adsorption (Table 3).

Table 3: Thermodynamic parameters of MA1 and MA2 in 1.0M HCl on the C38 steel at 298K.

ILs	R	K	$\Delta G^°_{ads}$ (kJ/mol)
MA1	0.99995	27663	-35.3
MA2	1	162338	-39.7

3.4. Surface morphology study

The surface morphologies of C-steel specimen in 1.0 M HCl solution free or containing some of the ILs inhibitors after 4 h immersion were examined using scanning electron microscopy (SEM) as displayed in Figures 7a–c. In the absence of inhibitors (Fig. 7a), a very rough surface was observed due to rapid corrosion attack of carbon steel by chloride anions. There are a large number of pits surrounded by iron oxide layer which almost fully covers the carbon steel surface, revealing that pit formation under these conditions occurs continuously during the exposure period while iron oxide builds up over the surface.

It is important to stress out that when ILs inhibitors (MA1and MA2) are present in the solution (Fig. 7b,c) the morphology of the carbon steel surface are quite different from the previous one and the rough surface (amount of the formed iron oxide and the number of pits) is visibly reduced indicating the formation of a protective film.
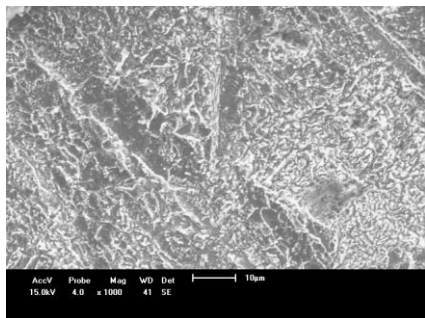
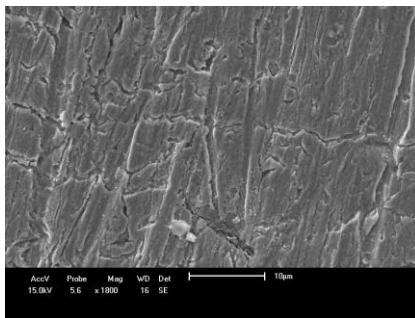**Figure 7a** SEM micrographs of the surface of the C-steel specimens in 1.0 M HCl.

Figure 7b SEM micrographs of the surface of the C-steel specimens in 1.0 M HCl in absence and in presence of10⁻² M of compound **MA1**.
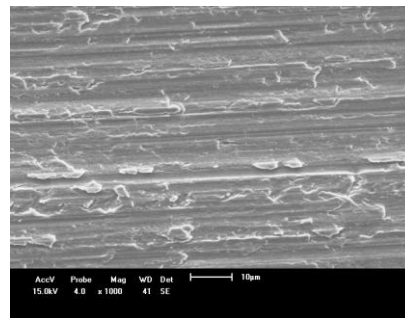
Figure 7c SEM micrographs of the surface of the C-steel specimens in 1.0 M HCl in absence and in presence of 10⁻² M of compound **MA2**.

3.5. Computational study

The aim of this part of our work is to investigate whether there is a clear relationship between the experimentally determined inhibition efficiencies of the studied inhibitors and a number of quantum-chemical parameters. Some of these parameters are directly extracted from the output files (E_{HOMO}, E_{LUMO}, μ)

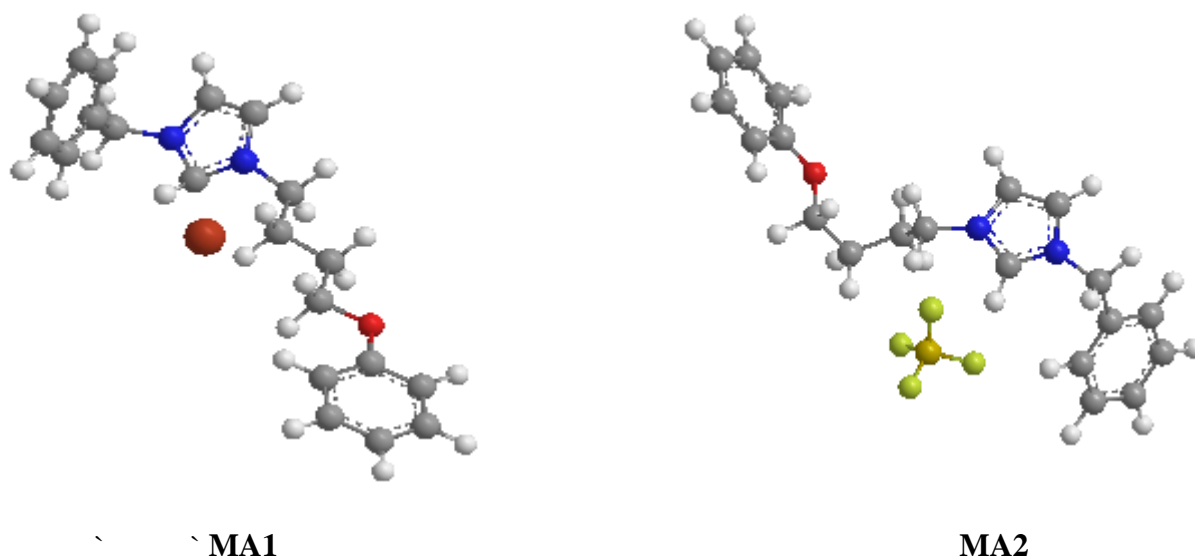`          `**MA1**   **MA2**

Fig 8. The optimized molecular structures of MA1 and MA2

The ILs MA1 and MA2 are investigated experimentally for their corrosion inhibitors properties. Quantum chemical calculations are developed to get more information on the more stable and performed molecular state in order to investigate the structural parameters which affect the inhibition efficiency of inhibitors and study their adsorption mechanisms on the metal surface.

These calculations permit also to get geometric and electronic structures of the inhibitors by optimizing of their bond lengths, bond angles and dihedral angles. Figure 8 present the optimized molecular structures of the studied inhibitors.

Table 4: Parameters Minimize Energy Computation of MA1 and MA2

J. Mater. Environ. Sci. 4 (5) (2013) 770-785   *Messali and Asiri*

ISSN : 2028-2508

CODEN: JMESCN

	MA1	MA2
Stretch	1.0850	1.3092
Bend	22.1482	96.4607
Stretch-Bend	-0.0810	-0.4269
Torsion	-11.2666	-10.9817
Non-1,4 VDW	1.4712	4.9297
1,4 VDW	13.0475	12.8913
Charge/Charge	-74.2422	-98.6945
Charge/Dipole	1.5803	1.2117
Dipole/Dipole	-0.4738	-0.4725
Total Energy (kcal/mol)	-46.7313	6.2269

The MM2 procedures described assume that we understand how the potential energy surface relates to conformations of our model. The MM2 atom type is used for force field calculations and used only in building models. Table 3 summarized all calculated parameters from the MM2 method, such as. Stretch, Bend, Stretch-Bend, Torsion, Non-1,4 VDW, 1,4 VDW , Charge/Charge , Charge/Dipole, Dipole/Dipole and Total Energy.

The theoretical calculation of the total partial charge density of Ionic liquids MA1 and MA2 (Figure 9) can reinforce the suggestion that the inhibitory effect contributed by the MA2 is greater than that provided by MA1.
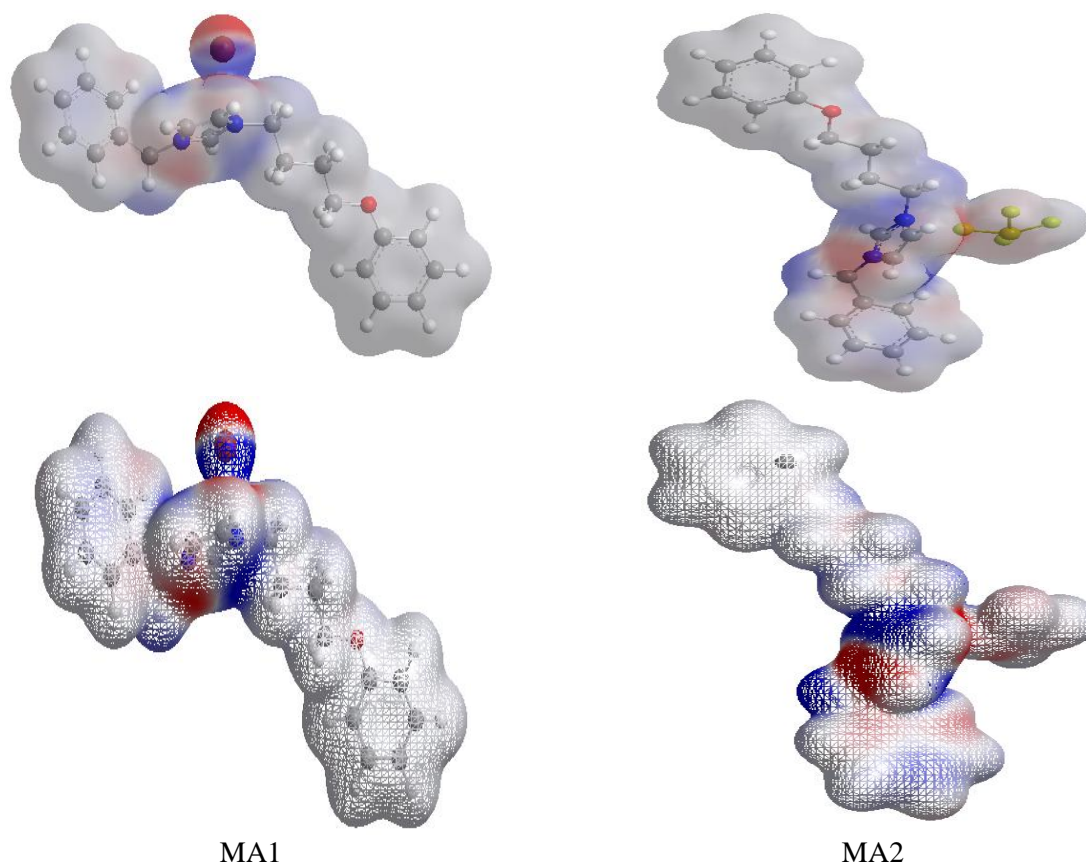.

MA1   MA2

Fig 9. Mulliken atomic charges of MA1 and MA2

The Mulliken charge density of MA1 and MA2 has been calculated and presented in Table 5. There is a general consensus by several authors that the more negatively charged heteroatom, the more it can be

adsorbed on the metal surface through donor-acceptor type reaction. From the values of Mulliken charge, there is an excess of negative charges in the Carbon atoms adjacent on nitrogen and oxygen atoms and heterocyclic groups, hence MA1 and MA2 molecules can be adsorbed on surface using these active centres leading to the corrosion inhibition effect.

Table 2: Mulliken charge of MA1 and MA2.

Number	Atom	Mulliken Charge of (MA1)	Mulliken Charge of (MA2)
1	N	-0.029784	-0.025023
2	C	-0.067120	-0.093286
3	C	-0.113166	-0.122321
4	N	-0.095322	-0.083285
5	C	0.046127	-0.010046
6	C	0.009299	0.015213
7	C	-0.121379	-0.122351
8	C	-0.116184	-0.110589
9	C	-0.118483	-0.131961
10	C	-0.115945	-0.105163
11	C	-0.123782	-0.130781
12	C	-0.128293	-0.100808
13	C	-0.003689	0.040792
14	C	-0.192548	-0.187703
15	C	-0.161908	-0.153336
16	C	-0.006277	-0.024487
17	C	-0.207523	-0.206101
18	O	0.092858	0.078463
19	C	-0.156705	-0.190184
20	C	-0.096190	-0.100060
21	C	-0.160666	-0.163622
22	C	-0.097569	-0.111438
23	C	-0.208867	-0.147234

The calculations which are responsible for the inhibition efficiency of inhibitors such as the energies of highest occupied molecular orbital (E_{HOMO}), energy of lowest unoccupied molecular orbital (E_{LUMO}), the separation energy ($E_{LUMO} - E_{HOMO}$), ΔE, representing the function of reactivity, the net charge on the functional group and dipole moment, μ, are collected in Table 4. The results seem to indicate that both the value of the gap energy ΔE, as well as the value obtained for the dipole moment, favor the (MA2) rather than (MA1), implying its effectiveness as a corrosion inhibitor.

The effectiveness of an inhibitor can be related to its spatial molecular structure, as well as with their molecular electronic structure. In addition, there are certain quantum chemical parameters that can be related to the interactions metal-inhibitor. Among these, we can mention the energy of the HOMO, which is often associated with the capacity of a molecule to donate electrons. Therefore, an increase in the values of E_{HOMO} can facilitate the adsorption and therefore the inhibition efficiency, by indicating the disposition of the molecule to donate orbital electrons to an appropriate acceptor with empty molecular orbitals. In the same way low values of the energy gap $\Delta E = E_{LUMO} - E_{HOMO}$ will render good inhibition efficiencies, since the energy needed to remove an electron from the last occupied orbital will be low. Similarly, low values of the dipole moment will favor the accumulation of inhibitor molecules on the metallic surface.

E_{HOMO} is a quantum chemical descriptor which is often associated with the electron donating ability of the molecule. High value of E_{HOMO} is likely to indicate a tendency of the molecule to donate electrons to appropriate acceptor molecule of low empty molecular orbital energy. Therefore, the

energy of the lowest unoccupied molecular orbital, E_{LUMO}, indicates the ability of the molecule to accept electrons. Therefore, the lower the value of E_{LUMO}, the more probable the molecule accepts electrons. The binding ability of the inhibitor to the metal surface increases with increasing the HOMO and decreasing the LUMO energy values.

The calculations show that ILs MA1 and MA2 have the highest HOMO level respectively at -0.35863 and -0.33389 a.u and the lowest LUMO level at 0.00518 and -0.03310 a. u. These results can explain that the highest inhibition efficiency of MA1 and MA2 molecule which are due to the increasing energy of the HOMO and the decreasing energy of the LUMO. This is in a good agreement with the experimental observations suggesting that ILs MA1 and MA2) have a high inhibition efficiency (Table 6).
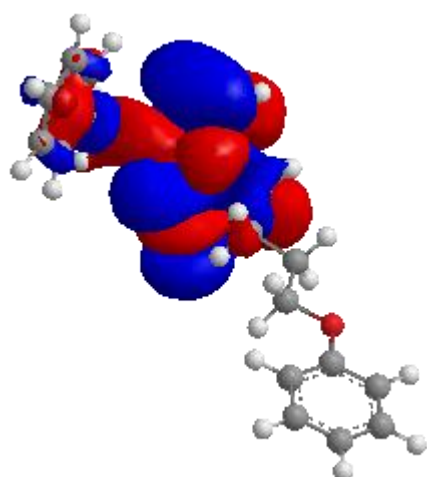
Table 6. the calculated quantum chemical parameters of the ILs MA1 and MA2

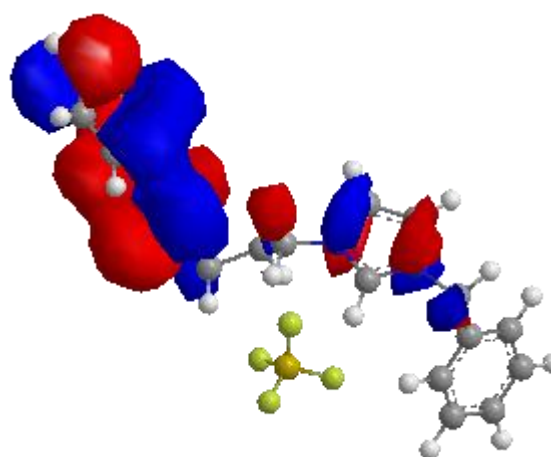| Inhibitors	HOMO (a. u)	LUMO (a. u)	ΔE (a. u)	E_{HF} (a. u)	μ (Debye)
MA1	-0.35863	0.00518	0.36381	0.0912002	0.495772
MA2	-0.33389	-0.03310	0.30079	-0.6220228	-0.630719

The separation energy, $\Delta E = (E_{LUMO} - E_{HOMO})$, is an important parameter as a function of reactivity of the inhibitor molecule towards the adsorption on metallic surface. As ΔE decreases, the reactivity of the molecule increases leading to increase in the inhibition efficiency of the molecule

It has been assumed that organic inhibitor molecules establish their inhibition action via the adsorption of the inhibitor onto the metal surface. The adsorption process is affected by the chemical structures of the inhibitors, the nature and charged surface of the metal and the distribution of charge over the whole inhibitor molecule. In general, two modes of adsorption can be considered.

Physical adsorption requires the presence of electrically charged metal surface and charged species in the bulk of the solution. Chemisorptions process includes charge sharing or charge transfer from the inhibitor molecule to the metal surface. The presence of the transition metal having vacant orbital of low energy with the inhibitor molecule having relatively loosely bound electrons or hetero atom with lone pair of electrons facilitates this adsorption

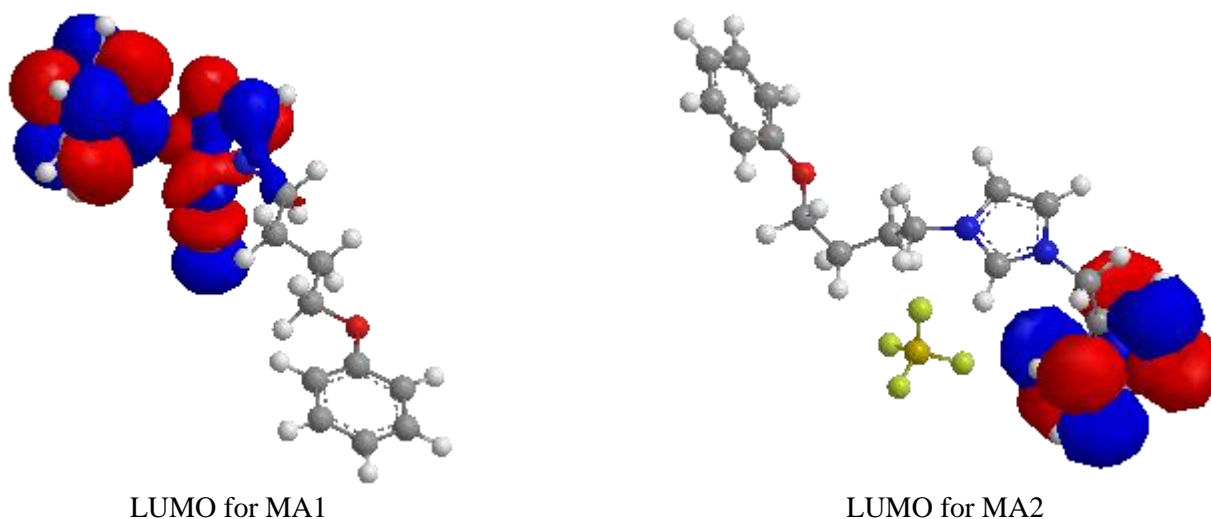HOMO for MA1   HOMO for MA2

LUMO for MA1   LUMO for MA2

Fig 10. The HOMO densities and LUMO densities for MA1 and MA2

We have demonstrated that there is a systematical change of the HOMO and LUMO energies into the ILs MA1 and MA2 causing a destabilisation for HOMO and LUMO levels and lowing the energy band gap. On the other hand, it will be useful to examine the HOMO and the LUMO for these studied molecules because the relative ordering of occupied and virtual orbital provides a reasonable qualitative indication of excitation properties and provides also the ability of electron hole transport. In general, and as plotted in Figure 10, the HOMO possesses an antibonding character between the consecutive subunits. On the other hand, the LUMO of all studied compounds generally shows a bonding character between the subunits.

4. Conclusion

From the overall experimental results and discussion the following conclusions can be deduced:

- Two new environmentally friendly imidazolium-based ionic liquids were prepared by using ultrasonic irradiation.
- Many advantages for the ultrasonic irradiation compared with the standard methods have been recorded.
- The tested ILs behaves as inhibitors for the corrosion of the C-steel in 1 M HCl solution.
- The inhibition is due to the adsorption of the inhibitor molecules on the C-steel surface and the blocking of active sites.
- Quantum chemical studies have been performed, using the B3LYP/6-31+G(d,p) method to investigate the properties of two newly synthesized ionic liquids and how their molecular properties relate to their ability to inhibit metal corrosion. A comparison of all the molecular properties suggests that MA1 is a better corrosion inhibitor than MA2. This result agrees well with the experimental inhibition efficiencies reported in the study, where, except for the results obtained at concentrations 10^{-2}M and 10^{-6}M, the corrosion inhibition efficiency of MA1 is higher than that of MA2.

Refrences
1. Lashkari M. and Arshadi, M.R. *Chemical Physics* 299 (2004) 131.
2. Zarrouk A. Dafali A., Hammouti B., Zarrok H., Boukhris S., Zertoubi M. *Int. J. Electrochem. Sci.* 5 (2010) 46

3. Zarrouk A., Chelfi, T., Dafali, A., Hammouti, B., Al-Deyab, S.S., Warad, I., Benchat, N., Zertoubi, M*., Int. J. Electrochem. Sci.* 5 (2010) 696.

4. Zarrouk A., Warad, I., Hammouti, B., Dafali, A., Al-Deyab, S.S., Benchat, N*., Int. J. Electrochem. Sci.* 5, (2010) 1516.

5. Hammouti B., Zarrouk, A., Al-Deyab, S.S., Warad, I. *Oriental J. Chem.* 27, (2011) 23.

6. Zarrouk A., Hammouti B., Dafali A., Zarrok H., *Der Pharm. Chem.* 3 (2011) 266.

7. Zarrouk A., Hammouti B., Touzani R., Al-Deyab, S.S., Zertoubi, M., Dafali, A., Elkadiri, S., *Int. J. Electrochem. Sci*. 6 (2011) 4939.

8. Zarrouk A., Hammouti B., Zarrok H., *Der Pharm. Chem.* 3 (2011) 263.

9. Zarrouk A., Hammouti B., Zarrok H., Al-Deyab S.S., Messali M., *Int. J. Electrochem. Sci*. 6 (2011) 6261.

10. Zarrok H., Saddik, R., Oudda, H., Hammouti, B., El Midaoui, A., Zarrouk A., Benchat, N., Ebn Touhami, M., *Der Pharm. Chem.* 3 (2011) 272.

11. Zarrok H., Oudda, H., Zarrouk, A., Salghi, R., Hammouti, B., Bouachrine, M*., Der Pharm. Chem.* 3 (2011) 576.

12. Zarrouk A., Hammouti, B., Zarrok, H., Bouachrine, M., Khaled, K.F., Al-Deyab, S.S., *Int. J. Electrochem. Sci*. 6 (2012) 89.

13. Zarrouk A, Hammouti, B., Zarrok, H., Salghi, R., Dafali, A., Bazzi, Lh., Bammou, L., Al-Deyab, S. S., *Der Pharm. Chem*. 4 (2012) 337.

14. Ghazoui A., Saddik, R., Benchat, N.,. Hammouti, B., Guenbour, M., Zarrouk, A., Ramdani, M., *Der Pharm. Chem*. 4 (2012) 352.

15. Zarrok H., Salghi, R., Zarrouk, A., Hammouti, B., Oudda, H., Bazzi, Lh., Bammou, L., Al-Deyab, S.S., *Der Pharm. Chem*. 4 (2012) 407.

16. Zarrok H., Oudda, H., El Midaoui, A., Zarrouk, A., Hammouti, B., Ebn Touhami, M., Attayibat, A., Radi, S., Touzani, R., *Res. Chem. Intermed*. (2012) DOI: 10.1007/s11164-012-0525-x).

17. Abd El-Maksoud S.A., Fouda, A.S., *Mater. Chem. Phys.* 93 (2005) 84.

18. Srikanth A.P., Sunitha, T.G., Raman, V., Nanjundan, S., Rajendran, N*., Mater. Chem. Phys.* 103 (2007) 241

19. Bouklah M., Attayibat A., Hammouti B., Ramdani A., Radi S., Benkaddour M., *Appl. Surf. Sci.* 240 (2005) 341

20. Rogers R.D., Seddon, K.R*., Science* 302 **(**2003) 792.

21. Jain N., Kumar, A., Chauhan, S., Chauhan, S.M.S., *Tetrahedron* 61 (2005), 1015.

22. Wilkes J.S., *Green Chem.* 4 (2002) 73.

23. Ngo H.L., LeCompte, K., Hargens, L., McEwen, A.B., *Thermochim. Acta* 357-358 (2000) 97.

24. Bonhôte P., Dias, A.-P., Papageorgiou, N., Kalyanasundaram, K., Gratzel, M. *Inorg. Chem.* 35 (1996) 1168.

25. Dieter K.M., Dymek, C.J., Heimer, N.E., Rovang, J.W., Wilkes, J.S., *J. Am. Chem. Soc*. 110 (1988) 2722.

26. Forsyth S.A., Pringle, J.M., MacFarlane, D.R., *Aust. J. Chem.* 57 (2004) 113.

27. Endres F., El Abedin, S.Z., Matter, S*., Phys. Chem. Chem. Phys*. 8 (2006) 2101.

28. Ibrahim M.AM., Messali M., 76 (2011), 14.

29. F. Al-Ghamdi A., Messali, M., Ahmed, S.A., *J. Mater. Environ. Sci.*, 2 (2011) 215.

30. Hagiwara R., Ito, Y., *J. Fluorine Chem.*, 105 (2000) 221.

31. Gasparac R., Martin, C.R., Stupnisek-Lisac, E., *J. Electrochem. Soc*. 147 (2000) 548.

32. Zhang D.Q., Gao, L.X., Zhu, G.D., *Corros. Sci.* 46 (2004) 3031.

33. Muralidharan S., Iyer, S.V.K*., Anti-Corros. Met. Mater*. 44 (1997) 100.

34. Shi S.C., Yi, P.G., Cao, C.Z., Wang, X.Y*., J. Chem. Ind. Eng. Chin*. 56 (2005) 1112.

35. Zhang Q.B., Hua, Y.X., *Electrochimica Acta* 54 (2009) 1881.

36. Ibrahim M.A.M., Messali, M., Moussa, Z., Alzahrani, A.Y., Alamry, S.N., Hammouti, B., *Portugaliae Electrochimica Acta,* 6 (2011) 375.

37. Messali M., *J. Mater. Environ. Sci*. 2 (2011) 174.

38. Zarrouk A., Messali M., Zarrok, H., Salghi, R., Al-Sheikh Ali, A., Hammouti, B., Al-Deyab, S. S., Bentiss, F., *Int. J. Electrochem. Sci.* 7 (2012) 6998.

39. Zarrouk A., Messali, M., Aouad, M.R., Zarrok, H., Salghi, R., Hammouti, B., Chetouani, A., Al-Deyab, S.S., *J. Chem. Pharm. Res.* 4 (2012) 3427.

40. Quraishi M.A., Rafiquee, M.Z.A., Khan, S., Saxena, N., *J. Appl. Electrochem*. 37 (2007) 1153.

41. Becke A.D., *J. Chem. Phys*. 96 (1992) 9489-9495.

42. Becke A.D., *J. Chem. Phys*. 98 (1993) 1372-1377.

43. C. Lee; W. Yang; R.G. *Parr.Phys. Rev. B*. 37(1988) 785-789.
44. Gaussian 03, Revision B.01, M. J. Frisch, et al., Gaussian, Inc., Pittsburgh, PA, 2003.
45. Anastas P. T.; Warner J. C.; Green Chemistry, Theory and Practice, Oxford University Press, Oxford, UK, 1998.
46. Loupy, A., *C. R. Chimie* 7 (2004)103.
47. Aupoix, A., Pegot, B., Vo-Thanh G., *Tetrahedron* 66 (2010) 1352.
48. Yi, F., Peng, Y., Song, G., *Tetrahedron Lett.* 46 (2005) 3931.
49. Singh, V., Kaur, S., Sapehiyia, V., Singh, J., Kad, G. L., *Catalysis Comm,* 6 (2005) 57.
50. Messali, M., Ahmed S.A., *Green and Sustainable Chemistry* 1 (2011) 70.
51. Messali, M., Moussa, Z., Alzahrani, A.Y., El-Naggar, M.Y., ElDouhaibi A.S., Hammouti, B., *Chemosphere,* 91 (2013) 1627
52. Ahamad I.; Prasad R.; Quraishi M.A., *Corros. Sci*. 52 (2010) 933-942.
53. Bentiss F.; Outirite M.; Traisnel M.; Vezin H.; Lagrenée M.; Hammouti B.; Al-Deyab S.S.; Jama C., *Int. J. Electrochem. Sci*. 7(2012) 1699-1723.
54. Khaled K.F., *Electrochim. Acta*. 48 (2003) 2493-2503.
55. Naderi E.; A.H. Jafari; M. Ehteshamzadeh; M.G. Hosseini. *Mater. Chem. Phys*. 113 (2009) 986-993.
56. Bentiss F.; Lebrini M.; Lagrenée M.; *Corros. Sci.* 47 (2005) 2915-2931.
57. Avci G., *Colloids Surf. A*. 317 (2008) 730-736.
58. Solmaz R.; Kardas G.; M. çulha, B. Yazici, M. Erbil. *Electrochim. Acta*. 53 (2008) 5941-5952.
59. Migahed M.A.; Nassar I.F.. *Electrochim. Acta*. 53 (2008) 2877-2882.